

SF Journal of Nanochemistry and Nanotechnology

Controllable Synthesis of Pure-Phase LaFeO₃ with Porous Structure and their Catalytic Performance for Pollutants Degradation

Humayun M^{1*}, Raziq F², Khan A³ and Ali F⁴

¹School of Optical and Electronic Information, Huazhong University of Science and Technology Wuhan, 430074, P.R. China

²School of Chemistry and Chemical Engineering, South China University of Technology, Guangzhou, 510640, P.R. China

³Department of Chemistry, Abdul Wali Khan University Mardan, 23200, Khyber Pakhtunkhwa, Pakistan

⁴Department of Chemistry, Hazara University Mansehra, 21300, Khyber Pakhtunkhwa, Pakistan

Abstract

In this work, we have successfully synthesized large scale controlled size porous LaFeO₃ (P-LFO) nanoparticles by sol-gel method using different amount carbon nanospheres (CNS) as a template. For comparison, we have also synthesized non-porous LaFeO₃ (NP-LFO) nanoparticles. Based on our experimental results, it is clearly demonstrated that the photocatalytic activity of P-LFO nanoparticles for phenol and rhodamine B degradation is significantly enhanced as compared to the NP-LFO. From BET results, it is confirmed that the amount of CNS greatly affect the surface area of the photocatalysts. The surface area of the as-prepared P-LFO nanoparticles is greatly improved especially with the used 0.2g CNS. Hence, it is suggested that the improved photocatalytic activity is well attributed to the increase in specific surface area of P-LFO. Moreover, it is demonstrated that this method could be extend to synthesize other metal-oxide nanoparticles with control size and large surface area. The as-prepared P-LFO nanoparticles might have potential applications in many fields such as catalysis, sensing, drug delivery and catalyst supports.

Keywords: P-LFO; Sol-gel method; Large surface area; Phenol degradation; Rhodamine B degradation

Introduction

Nanomaterials with control morphology are of enormous scientific and technological interest nowadays [1]. Generally, the materials properties can remarkably turnover from the introduction of various nanosized dimensions to their structures. Usually, the most resourceful technique for tuning the morphology of nanomaterials is soft and hard templating. The size and shape of nanostructured or porous materials can easily be tuned by choosing templates with appropriate structures [2]. The templates acts as structure directing agents at a given length scale in order to obtain nanomaterials with hierarchical porous structure. Materials with porous structure have many applications such as charge transport at multiple scales, high surface areas and can also provide short diffusion paths intrinsic to nanosized features and to facilitate interfacial charge transport in heterojunctions [3]. Therefore, it is highly desirable to develop an effective strategy to synthesize materials with porous morphology [4]. Although, there have been published a lot of works about the synthesis of porous nanomaterials with the aid of soft and hard templates. Among them, surfactant-assisted PMMA-templating [5], polystyrene colloidal crystal template [6,7,8], Phase-transformable emulsions composed of natural beeswax as templates [9] and Triblock copolymer surfactant P123 assisted template [10] have been widely investigated.

Perovskite-type oxide nanomaterials with general formula ABO₃ have attracted tremendous attention in the present decade because of their potential applications in the field of photocatalysis, superconductors, electrocatalysis, pollutants oxidation, chemical sensors, photolysis of water molecules, etc [11]. In perovskite oxides, the B-site cation is smaller in diameter and six-fold coordinated by oxygen anions while site A is bigger and twelve-fold coordinated by oxygen anions. In ABO₃ crystal lattice, the BO₆ octahedral units share their vertexes with each other to form crystal structure back bone while the A cations occupy interstitial spaces between the octahedral units [12].

OPEN ACCESS

*Correspondence:

Muhammad Humayun, School of Optical and Electronic Information, Huazhong University of Science and Technology Wuhan, 430074, P.R. China.

Tel: +86-15-776432167

E-mail: humayun096@yahoo.com

Received Date: 09 Nov 2017

Accepted Date: 20 Jan 2018

Published Date: 27 Jan 2018

Citation: Humayun M, Raziq F, Khan A, Ali F. Controllable Synthesis of Pure-Phase LaFeO₃ with Porous Structure and their Catalytic Performance for Pollutants Degradation. SF J Nanochem Nanotechnol. 2018; 1(1): 1001.

ISSN 2643-8135

Copyright © 2018 Humayun M. This is an open access article distributed under the Creative Commons Attribution License, which permits unrestricted use, distribution, and reproduction in any medium, provided the original work is properly cited.

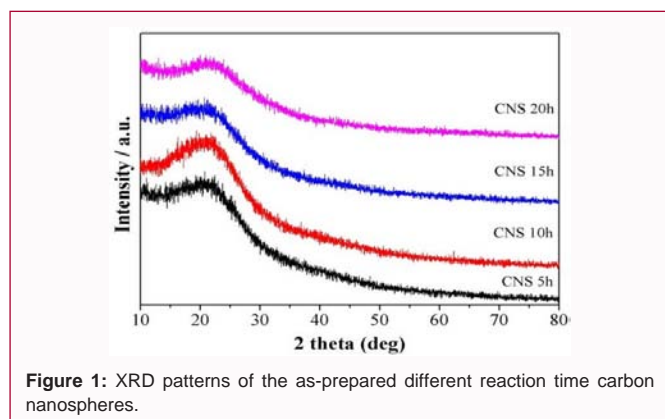


Figure 1: XRD patterns of the as-prepared different reaction time carbon nanospheres.

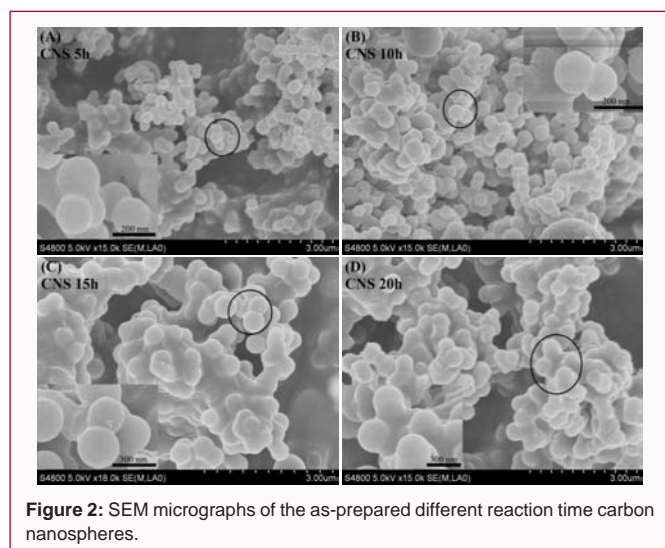


Figure 2: SEM micrographs of the as-prepared different reaction time carbon nanospheres.

In ABO_3 -based oxides, the B-site cations are of great importance, because of its potential for redox reactions. Generally, it is obvious that ABO_3 -type perovskites have potential applications in the field of catalysis. Among the known ABO_3 perovskites, $LaFeO_3$ has mostly been investigated because of its potential applications in solid oxide fuel cells, electronic and magnetic materials, gas sensors, photo and electrocatalysis. Due to its narrow bandgap (2.0 eV), $LaFeO_3$ can be regarded as visible-light driven photocatalyst. Unfortunately, $LaFeO_3$ exhibit low photocatalytic activity which is attributed to the low surface area. In order to make the material more valuable for practical applications, the material with control morphology and porous structure that impart greater catalytic efficiency is highly desirable [13].

Herein, we report the synthesis of porous $LaFeO_3$ nanoparticles by sol-gel method using carbon nanospheres as a hard template. For comparison, we have also synthesized non-porous $LaFeO_3$ nanoparticles. It is clearly demonstrated by means of experimental results, that the photocatalytic activity of P-LFO nanoparticles for phenol and Rhodamine B degradation is obviously enhanced as compared to the NP-LFO. The increase in surface area of P-LFO material is confirmed by the N_2 adsorption/desorption isotherms. Moreover, it is investigated that the amount of CNS greatly affects the surface area of the photocatalysts. The surface area of the as-prepared P-LFO nanoparticles is greatly improved especially with the used 0.2 g CNS. Hence, it is suggested that the improved photocatalytic activity is well attributed to the increase in specific surface area of

Table 1: BET surface area and pore volume.

S.#	Samples	BET Surface Area ($m^2 \cdot g^{-1}$)	Pore volume $cm^3 \cdot g^{-1}$ (STP)
01	NP-LFO	5.4005	0
02	P- LFO CNS-0.05g	16.9776	0.076603
03	P- LFO CNS-0.1g	17.2164	0.103504
04	P- LFO CNS-0.2g	23.8963	0.125281
05	P- LFO CNS-0.4g	18.2976	0.069128

P-LFO due to porous structure. This work will provide feasible routes to synthesize porous nanomaterials with control morphology for potential applications in photocatalysis.

Experimental Section

Chemicals and reagents

All the reagents were of analytical grade and used as received without further purification.

Deionized water was used throughout the experiment.

Materials synthesis

Synthesis of carbon nanospheres: The first step involved the synthesis of carbon nanospheres with different diameters controlled by the reaction time (i.e. 5h, 10h, 15h and 20h) under the hydrothermal condition at $180^\circ C$. For each sample, 4g of D-glucose was taken and dissolved into 80mL of deionized water under continuous stirring. The solutions were transferred to 100mL of Teflon-lined stainless steel autoclaves and hydrothermally treated at $180^\circ C$ for 5, 10, 15 and 20h respectively. After cooling to room temperature naturally, the black product was centrifuged and washed several times with deionized water followed by absolute ethanol and finally dried in oven at $60^\circ C$ for 12h.

Synthesis of non-porous and porous $LaFeO_3$ nanoparticles: Non-porous $LaFeO_3$ (NP-LFO) nanoparticles were synthesized by taking equimolar (1.5 mol) amounts of $La(NO_3)_3 \cdot 6H_2O$ and $Fe(NO_3)_3 \cdot 9H_2O$ and dissolved into a mixed solvent of ethylene glycol (EG) and deionized water (25mL+25mL) at room temperature. The metal nitrate solution was kept under vigorous stirring for 3h. After that, the solution was dried in convection oven at $80^\circ C$ for 24h. The dry powder was calcined in air at $600^\circ C$ ($5^\circ C \cdot min^{-1}$) for 2h to obtain non-porous $LaFeO_3$ nanoparticles. Porous $LaFeO_3$ nanoparticles were obtained by the same procedure but to the metal nitrate precursor solutions, different amount (0.05g, 0.1g, 0.2g and 0.4g) of carbon nanospheres were added and well dispersed with the assistance of sonication for 1h. To remove carbon nanospheres, the product was annealed at $400^\circ C$ with a temperature ramp of $1^\circ C \cdot min^{-1}$ for 2h and then annealed at $600^\circ C$ ($5^\circ C \cdot min^{-1}$) for another 2h.

Materials characterization

The materials were characterized by various techniques. The crystal structures of the samples were determined with the help of XRD (Rigaku D/MAX-rA powder diffractometer, Japan), using $Cu K\alpha$ radiation ($\lambda = 0.15418nm$), at an accelerating voltage of 30 kV, and emission current of 20mA was employed. The UV-vis diffuse reflectance spectra (UV-vis DRS) of the samples were recorded with Shimadzu UV-2550 Spectrophotometer, using $BaSO_4$ as a reference. Scanning electron microscopy (SEM) images were taken using a Hitachi S-4800 instrument (Tokyo, Japan), operating at acceleration voltage of 15kV. Transmission electron microscopy (TEM) images were taken by a JEM-3010 electron microscope

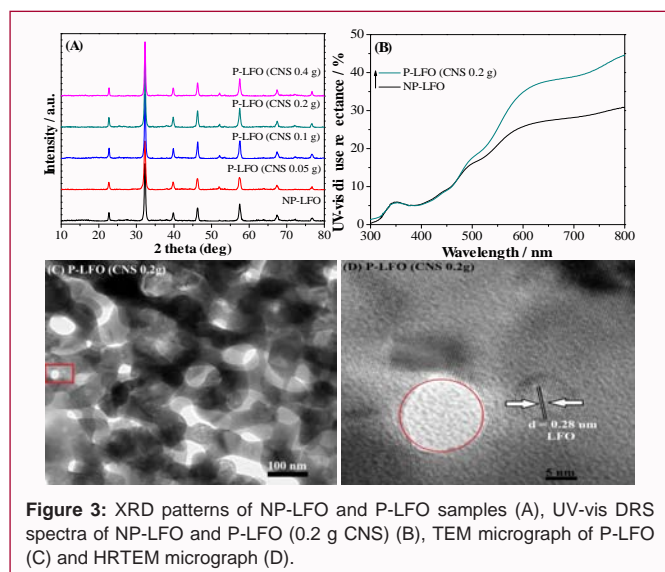


Figure 3: XRD patterns of NP-LFO and P-LFO samples (A), UV-vis DRS spectra of NP-LFO and P-LFO (0.2 g CNS) (B), TEM micrograph of P-LFO (C) and HRTEM micrograph (D).

(JEOL, Japan), operated at an acceleration voltage of 300 kV. The N_2 adsorption-desorption isotherm of various samples were carried out by Micromeritics ASAP 2020M system at the temperature of liquid nitrogen, while keeping the system out-gassed for 10h at 300°C prior to measurements. ST-2000 constant volume adsorption apparatus was used for the evaluation of BET surface area.

Evaluation of photocatalytic activity for pollutants degradation

Rhodamine B (RhB) dye and phenol widely exists in industrial production are potentially toxic and carcinogenic and are harmful to human health and the environment. Thus, both were chosen as model pollutants to evaluate the photocatalytic activity of P-LFO samples. During the photocatalytic degradation experiments of RhB, 0.1g of the as-prepared sample was added to 40mL of 10mgL⁻¹ RhB solution. The solution was stirred for 30min in dark, in order to reach the adsorption equilibrium. Then, the solution was irradiated for 1h under continuous stirring. After that, the solution was centrifuged and the RhB concentration was analyzed by means of the characteristic optical absorption at 553nm with a Model Shimadzu UV2550 spectrophotometer. The photocatalytic experiments for phenol degradation were carried out in 100mL open photochemical glass reactor and irradiation was provided from a side of the reactor using a 150W GYZ220 high-pressure Xenon lamp made in China with a 420nm cutoff wavelength filter, which was placed at about 10 cm distance from the reactor. During the photocatalytic degradation of phenol, 0.1g of photocatalyst and 80mL of 10mg/L phenol solution were mixed by a magnetic stirrer for 0.5h to reach the adsorption saturation and then begin to irradiate. After photocatalytic reaction for 1h, the phenol concentration was analyzed by the colorimetric method of 4-aminoantipyrine at the characteristic optical adsorption of 510nm with a Model Shimadzu UV-2550 spectrophotometer after centrifugation.

Measurement of the produced hydroxyl radical (\cdot OH) amount

In the analysis of hydroxyl radicals, 50mg sample and 20mL of 5mg/L⁻¹ coumarin aqueous solution were mixed in a 50mL quartz reactor under vigorous stirring. A 150W high-pressure Xenon lamp as its irradiation source with a cutoff filter ($\lambda > 420$ nm) was placed at about 10cm from the reactor and the sample was irradiated for 1h.

After centrifugation, a certain amount of the solution was transferred into a Pyrex glass cell for the fluorescence measurement of 7-hydroxycoumarin under the excitation wavelength of 350nm.

Results and Discussion

The first step involved the synthesis of controllable size carbon nanospheres (CNS) with different diameters controlled by the reaction time (i.e. 5h, 10h, 15h and 20h) under the hydrothermal condition at 180°C. Figure 1 shows the XRD patterns of the as-prepared carbon nanospheres. The XRD patterns of all samples exhibit a broad peak at $2\theta = 20$, which is the characteristic peak of graphitic carbon.

The morphology of the as-prepared different reaction time CNS is investigated by SEM analysis as shown in Figure 2. The diameter of the CNS falls in the range of 200–300nm. The CNS obtained with 5h reaction time has uniform morphology with a diameter of approximately 200nm, therefore selected as a hard template for the synthesis of P-LFO nanoparticles.

The crystal structure and phase purity of perovskite-type NP-LFO and the P-LFO photocatalysts prepared with different amount of CNS were investigated by X-ray diffraction (XRD) as depicted in Figure 3A. The XRD patterns of NP-LFO and P-LFO samples calcined at 600°C exhibit diffraction peaks, which are the characteristic of highly crystalline product. These peaks are well-indexed to the orthorhombic phase of perovskite type $LaFeO_3$ with *pnma* space group and are consistent with the standard pattern of JCPDS card no. 88-0641, without any impurity phase [14,15]. According to the previous literature [16], the orthorhombic phase can transfer the excited energy of the photogenerated charge carriers (electron-hole pairs) very efficiently. In other words, the orthorhombic structure of the as-prepared samples is favorable for the separation of electrons and holes, which is beneficial for photocatalytic reactivity [17]. In order to explore the optical properties of the as-prepared samples, UV-visible diffuse reflectance spectroscopy (UV-vis DRS) measurements of NP-LFO and the P-LFO (0.2g CNS) photocatalysts were performed as shown in Figure 3B. It can be seen that both the samples show an

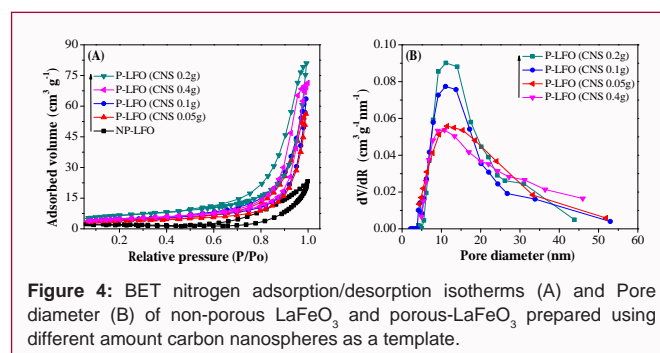


Figure 4: BET nitrogen adsorption/desorption isotherms (A) and Pore diameter (B) of non-porous $LaFeO_3$ and porous- $LaFeO_3$ prepared using different amount carbon nanospheres as a template.

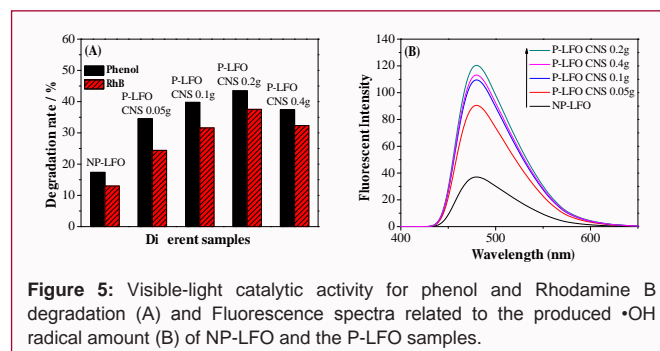


Figure 5: Visible-light catalytic activity for phenol and Rhodamine B degradation (A) and Fluorescence spectra related to the produced \cdot OH radical amount (B) of NP-LFO and the P-LFO samples.

absorption edge at about 620nm, which is attributed to its electronic transition from the valance band to conduction band ($O2p \rightarrow Fe3d$), and the optical absorption across the energy band gap is calculated to be 2.0eV, based on the energy band gap equation $E_g = 1240/\lambda_g$ (eV) [13,18,19]. The morphology of as-prepared P-LFO sample is investigated by TEM analysis. From TEM image (Figure 3C), it is clear that the sample exhibit porous structure. From HRTEM image (Figure 3D), it is clear that the pore exhibit diameter in the range of 10-15nm and the lattice fringes with d-spacing of 0.28nm correspond to LFO [20].

Nitrogen adsorption/desorption isotherms

The specific surface area and the pore size distribution of NP-LFO and P-LFO photocatalysts were determined by N_2 adsorption-desorption isotherm measurements as shown in Figure 4A and 4B respectively. It can be observed that all the P-LFO samples exhibit hysteresis loops in the high relative pressure region indicating the formation of porous structure. Based on the Brunauer-Emmett-Teller (BET) method, it is investigated that NP-LFO exhibit a specific surface area $5.4005m^2.g^{-1}$, while the P-LFO samples synthesized with different amount CNS exhibit rather higher specific surface area (i.e. 16.9776, 17.2164, 23.8963 and $18.2976m^2.g^{-1}$ respectively) as shown in Table 1. The pore size distribution of the photocatalysts was determined by Barrett-Joyner-Halenda (BJH) analysis. According to the BJH analysis, the P-LFO samples display ultra large pore volume (i.e. 0.076603, 0.103504, 0.125281 and $0.069128cm^3.g^{-1}$) at predetermined P/P^0 [21,22]. From BET results, it is concluded that the over excess amount of CNS decrease the surface area and pore volume of the as-prepared P-LFO photocatalysts. This may be attributed to the aggregation of CNS in the precursor solution. The average pore size diameter of P-LFO falls in the range of 10-15nm which is consistent with TEM results.

Visible-light photoactivities

The visible-light photocatalytic activities of NP-LFO and P-LFO photocatalysts were evaluated for RhB and phenol degradation. From Figure 5A, it can be observed that NP-LFO does not show obvious activity for RhB and phenol degradation. However, an obvious increase in photocatalytic activity is observed for P-LFO photocatalysts. Interestingly, the P-LFO photocatalyst (CNS 0.2g) exhibit the best photoactivity for RhB and phenol degradation. This is mainly attributed to greatly increase specific surface area due to porous structure and oxygen adsorption concentration. Hence, it is suggested that when surface area of the photocatalyst increases, more O_2 could be adsorbed on the surface which capture the photogenerated electrons in the conduction band for reduction reactions while the induced holes in the valance band reacts with water to produce hydroxyl radicals that proceed oxidation reactions. To further prove this, coumarin fluorescent method was used to measure the $\bullet OH$ species amount as depicted in Figure 5B. It is widely accepted that $\bullet OH$ species play a vital role in catalysis for the photocatalytic degradation of various pollutants [23,24]. From the fluorescence spectra, it is concluded that the NP-LFO shows low $\bullet OH$ radical amount, however, a significant increase in $\bullet OH$ radical amount is observed for P-LFO photocatalysts especially for the P-LFO with the used 0.2 g CNS. From the above results, it is concluded that the enhanced visible-light photocatalytic activity of P-LFO for RhB and phenol degradation is attributed to the significant increase in amount of $\bullet OH$ radicals produced.

Conclusion

Based on the above results, it is concluded that controllable size large surface area porous nanomaterials could be obtained by using carbon nanospheres a hard template. The introduction of porous structure will greatly improve the efficiency of nanomaterials. This work will provide feasible strategies to synthesize nanophotocatalysts with large surface area for potential applications in photocatalysis.

References

- Haisheng Qian, Guofeng Lin, Yunxia Zhang, Poernomo Gunawan and Rong Xu. A new approach to synthesize uniform metal oxide hollow nanospheres via controlled precipitation. *Nanotechnol.* 2007; 18: 355602.
- Arne Thomas, Frederic Goettmann, and Markus Antonietti. Hard Templates for Soft Materials: Creating Nanostructured Organic Materials. *Chem. Mater.* 2008; 20: 738-755.
- Andreas Stein, Stephen G. Rudisill, and Nicholas D. Petkovich. Perspective on the Influence of Interactions Between Hard and Soft Templates and Precursors on Morphology of Hierarchically Structured Porous Materials. *Chem. Mater.* 2014; 26: 259-276.
- Yuxi Liu, Hongxing Dai, Jiguang Deng, Lei Zhang, Baozu Gao, Yuan Wang, et al. PMMA-templating generation and high catalytic performance of chain-like ordered macroporous $LaMnO_3$ supported gold nanocatalysts for the oxidation of carbon monoxide and toluene. *Appl. Catal.* 2013; B 140: 317-326.
- Zhenxuan Zhao, Hongxing Dai, Jiguang Deng, Yucheng Du, Yuxi Liu and Lei Zhang. Three-dimensionally ordered macroporous $La_{0.6}Sr_{0.4}FeO_{3-\delta}$: High-efficiency catalysts for the oxidative removal of toluene. *Microporous. Mesoporous. Mater.* 2012; 163: 131-139.
- Min Zhou, Jian Bao, Yang Xu, Jiajia Zhang, Junfeng Xie, Meili Guan, et al. Photoelectrodes Based upon Mo: $BiVO_4$ Inverse Opals for Photoelectrochemical Water Splitting. *ACS Nano.* 2014; 8: 7088-7098.
- Min Zhou, Hao Bin Wu, Jian Bao, Lin Liang, Xiong Wen (David) Lou and Yi Xie. Ordered Macroporous $BiVO_4$ Architectures with Controllable Dual Porosity for Efficient Solar Water Splitting. *Angew. Chem.* 2013; 125: 8741-8745.
- Ji-Jing Xu, Zhong-Li Wang, Dan Xu, Fan-Zhi Meng and Xin-Bo Zhang. 3D ordered macroporous $LaFeO_3$ as efficient electrocatalyst for Li- O_2 batteries with enhanced rate capability and cyclic performance. *Energy Environ. Sci.* 2014; 7: 2213-2219.
- Zhenxuan Wang, Min Chen, and Limin Wu. Synthesis of Monodisperse Hollow Silver Spheres Using Phase-Transformable Emulsions as Templates. *Chem. Mater.* 2008; 20: 3251- 3253.
- Haiyan Jiang, Xue Meng, Hongxing Dai, Jiguang Deng, Yuxi Liu, Lei Zhang, et al. High-performance porous spherical or octapod-like single-crystalline $BiVO_4$ photocatalysts for the removal of phenol and methylene blue under visible-light illumination. *J. Hazard. Mater.* 2012; 217: 92-99.
- Xiang Liu and Karl Sohlberg. Theoretical calculations on layered perovskites: implications for photocatalysis. *Complex Met.* 2014; 1: 103-121.
- K. Momma and F. Izumi. VESTA 3 for three-dimensional visualization of crystal, volumetric and morphology data. *J. Appl. Cryst.* 2011; 44: 1272-1276.
- Muhammad Humayun, Zhijun Li, Liqun Sun, Xuliang Zhang, Fazal Raziq, Amir Zada, et al. Coupling of Nanocrystalline Anatase TiO_2 to Porous Nanosized $LaFeO_3$ for Efficient Visible-Light Photocatalytic Degradation of Pollutants. *Nanomaterials.* 2016; 6: 22; doi:10.3390/nano6010022.
- Saumitra N Tijare, Meenal V Joshi, Priyanka S Padole, Priti A Mangrulkar, Sadhana S Rayalu and Nitin K Labhsetwar. Photocatalytic hydrogen generation through water splitting on nano-crystalline $LaFeO_3$ perovskite. *Int. J. Hydrog. Energy.* 2012; 37: 10451-10456.

15. Y Wang, J Zhu, L Zhang, X Yang, X Wang, et al. Preparation and characterization of perovskite LaFeO₃ nanocrystals. *Mater. Lett.* 2006; 60: 1767–1770.
16. H Kato and A Kudo. Photocatalytic water splitting into H₂ and O₂ over various tantalate photocatalysts. *Catal. Today.* 2003; 78: 561–569.
17. Kun Gao and Shudan Li. Multi-modal TiO₂-LaFeO₃ composite films with high photocatalytic activity and hydrophilicity. *Appl. Surf. Sci.* 2012; 258: 6460–6464.
18. Fazal Raziq, Liqun Sun, Yuying Wang, Xuliang Zhang, Muhammad Humayun, Sharafat Ali, et al. Synthesis of Large Surface-Area g-C₃N₄ Comodified with MnOx and Au-TiO₂ as Efficient Visible-Light Photocatalysts for Fuel Production. *Adv. Energy Mater.* 2017; 1701580; doi: 10.1002/aenm.201701580.
19. Muhammad Humayun, Amir Zada, Zhijun Li, Mingzheng Xie, Xuliang Zhang, Yang Qu, et al. Enhanced visible-light activities of porous BiFeO₃ by coupling with nanocrystalline TiO₂ and mechanism. *Appl. Catal. B.* 2016; 180: 219–226.
20. Muhammad Humayun, Yang Qu, Fazal Raziq, Rui Yan, Zhijun Li, Xuliang Zhang, et al. Exceptional Visible-Light Activities of TiO₂-Coupled N-Doped Porous Perovskite LaFeO₃ for 2,4-Dichlorophenol Decomposition and CO₂ Conversion. *Environ. Sci. Technol.* 2016; 50: 13600-13610.
21. Peng Song, Huihui Zhang, Dan Han, Jia Li, Zhongxi Yang and Qi Wang. Preparation of biomorphic porous LaFeO₃ by sorghum strawbiotemplate method and its acetone sensing properties. *Sens. Actuators B.* 2014; 196: 140–146.
22. Jing Zhao, Yiping Liu, Xiaowei Li, Geyu Lu, Lu You, Xishuang Liang, et al. Highly sensitive humidity sensor based on high surface area mesoporous LaFeO₃ prepared by a nanocasting route. *Sens. Actuators B.* 2013; 181: 802–809.
23. Fazal Raziq, Yang Qu, Xuliang Zhang, Muhammad Humayun, Jing Wu, Amir Zada, et al. Enhanced Cocatalyst-free Visible-light Activities for Photocatalytic Fuel Production of g-C₃N₄ by Trapping Holes and Transferring Electrons. *J. Phys. Chem. C.* 2016; 120: 98–107.
24. Lumei He, Liqiang Jing, Yunbo Luan, Lei Wang and Honggang Fu. Enhanced Visible Activities of α-Fe₂O₃ by Coupling N-Doped Graphene and Mechanism Insight. *ACS Catal.* 2014; 4: 990–998.